



HAL
open science

The effect of the cutoff frequency on the sound production of a clarinet-like instrument

E Petersen, P. Guillemain, J. Kergomard, T Colinot

► **To cite this version:**

E Petersen, P. Guillemain, J. Kergomard, T Colinot. The effect of the cutoff frequency on the sound production of a clarinet-like instrument. *Journal of the Acoustical Society of America*, 2019, 10.1121/1.5111855 . hal-02188757

HAL Id: hal-02188757

<https://hal.science/hal-02188757>

Submitted on 26 Jul 2019

HAL is a multi-disciplinary open access archive for the deposit and dissemination of scientific research documents, whether they are published or not. The documents may come from teaching and research institutions in France or abroad, or from public or private research centers.

L'archive ouverte pluridisciplinaire **HAL**, est destinée au dépôt et à la diffusion de documents scientifiques de niveau recherche, publiés ou non, émanant des établissements d'enseignement et de recherche français ou étrangers, des laboratoires publics ou privés.

The effect of the cutoff frequency on the sound production of a clarinet-like instrument

E. Petersen,¹ P. Guillemain,¹ J. Kergomard,¹ and T. Colinot¹

Aix Marseille Univ, CNRS, Centrale Marseille, LMA, UMR 7031, Marseille, France^{a)}

1 The input impedance of woodwind instruments is characterized by at least two bands
2 due to the lattice of open toneholes, a stop band at low frequencies and a pass band
3 at higher frequencies where the acoustic energy is able to propagate past the first
4 open tonehole and into the lattice. The cutoff frequency that separates these two
5 bands is an approximate value that is determined by the geometry of the lattice of
6 open toneholes. It is expected that the frequency at which the stop band transitions
7 to the pass band affects the sound produced by the instrument, but it is not known
8 how this frequency affects the competition between self-sustained oscillation and ra-
9 diation. A simplified model of a clarinet-like resonator is conceived such that the
10 first input impedance peak and the cutoff frequency can be independently chosen.
11 Experimental prototypes are built and their measured impedance are compared with
12 the simulations. Resonators with very similar low frequency behavior, but very dif-
13 ferent cutoff frequencies, are then compared using digital synthesis to evaluate the
14 influence of the cutoff frequency on sound production. The cutoff frequency impacts
15 the synthesized pressure and acoustic volume velocity in the mouthpiece, particularly
16 regarding the spectral content at high frequencies.

^{a)}petersen@lma.cnrs-mrs.fr;

17 I. INTRODUCTION

18 Reed instruments are typically characterized by two main components: the reed and flow
19 rate as a nonlinear excitation mechanism and the main bore of the instrument as a passive
20 acoustic resonator that responds to and influences the excitation mechanism. Under normal
21 playing conditions the resonator responds to an injection of acoustical energy from the
22 exciter by radiating sound, but also facilitates the self-sustained oscillation of the exciter.¹
23 The input impedance, determined by the specific geometry of the bore and tonehole network,
24 is a standard way to characterize the acoustic behavior of the resonator. A resonator with
25 a series of open toneholes exhibits a well-known behavior called the tonehole lattice cutoff
26 frequency, below which a lattice wave sampled at discrete points is evanescent, while above, a
27 lattice wave can propagate further into the bore.^{2,3} Below the cutoff frequency the resonator
28 has an effective length that is approximately the length between the input and the first open
29 tonehole. In the case of a cylindrical bore, due to constructive interference of the reflected
30 waves, the input impedance is characterized by well-defined, nearly harmonically spaced
31 maxima expected of a quarter-wave resonator. Above the cutoff frequency, the effective
32 length of the resonator is a complicated function of frequency, so there is less organized
33 constructive and destructive interference, and the impedance is characterized by attenuated
34 peaks that are not harmonically related to the first impedance peak.

35 It is often assumed that the cutoff frequency behavior is related to the perceptual char-
36 acteristics of the sound produced by an instrument.^{1,4} However, it is not known precisely
37 in what way the cutoff frequency affects the production and radiation of sound. Therefore,

38 it is worth investigating how the frequency at which cutoff occurs, and the severity of the
39 cutoff behavior on the input impedance, could impact the self-sustained oscillation and the
40 temporal and spectral characteristics of the produced sound. Similarly, the cutoff frequency
41 may impact characteristics of sound radiation such as directivity and total radiated power
42 with respect to frequency. The complicated behavior associated with sound production and
43 radiation are linked to one another through the competition between the acoustical energy
44 that is retained within the resonator, which facilitates production, and that which is radiated
45 into the surrounding environment.

46 The goal of this article is to evaluate how the cutoff frequency impacts different aspects of
47 sound production and timbre features. To reduce the number of parameters that influence
48 the acoustical behavior of a real instrument, the current work (except Sect. III C) considers
49 resonators composed of a cylindrical main bore terminated by a lattice of geometrically reg-
50 ularly spaced toneholes. This simplified version of a clarinet resonator allows direct analysis
51 of the effects of the cutoff frequency without added complications such as irregular tone-
52 hole lattices, conical segments, and undercut toneholes, as is the case for actual woodwind
53 instruments.

54 Section II contains a review of the Transfer Matrix Method (TMM)⁵⁻⁷ for simulating
55 the input impedance of a pipe, including the related Transfer Matrix Method with exter-
56 nal Interactions (TMMI),⁸ which accounts for mutual radiation impedance when there are
57 more than a single radiating aperture (toneholes and open termination of the main bore).
58 Section III details the design and experimental verification of a cylinder and tonehole lattice
59 resonator for which it is possible to specify both the frequency of the first impedance peak

60 and the cutoff frequency. The effects on sound production, for three different resonators,
 61 are compared using digital synthesis in Section IV. The main focus of this section is to
 62 characterize the internal sound field, as well as the transfer function between internal and
 63 radiated time averaged intensity. Examples of synthesized pressure and velocity waveforms
 64 are furnished as supplementary materials online. Conclusions and proposals for future work
 65 are covered in Section V.

66 II. INPUT IMPEDANCE CALCULATIONS VIA THE TRANSFER MATRIX 67 METHOD WITH EXTERNAL INTERACTIONS

68 While the TMM is elegant, simple, and efficient, it ignores the effects of external interac-
 69 tions due to toneholes radiating simultaneously into the same space. A variant of the TMM
 70 is the Transfer Matrix Method with external Interactions (TMMI).^{8,9} This method accounts
 71 for propagation within the main bore while also accounting for the mutual impedance be-
 72 tween apertures (N toneholes and the bore end) that are assumed to radiate into the same
 73 space, and therefore have a mutual influence.

74 The TMMI allows the calculation of the acoustic pressure vector P and the acoustic flow
 75 vector U through each aperture of the resonator. They are related to the source term by

$$U = [\mathbb{I} + \mathbb{Y}(\mathbb{Z} + \mathbb{B})]^{-1}U^s \tag{1}$$

$$P = \mathbb{Y}^{-1}(U^s - U),$$

76 where U^s is the source vector, of dimension $N + 1$ and with only one non zero element:
 77 $U_n^s = \delta_{n,1}$. \mathbb{I} is the identity matrix, and \mathbb{Y} is a tri-diagonal admittance matrix, derived
 78 from the 2x2 transfer matrices of the main bore between toneholes. A cylinder is added to

79 account for the section of pipe separating the mouthpiece from the first open tonehole of
 80 a real instrument. \mathbb{B} is the impedance matrix for the acoustic mass of each tonehole: the
 81 definition includes many equations, and can be found in the appendix of Lefebvre *et al.*⁸
 82 \mathbb{Z} is the radiation impedance matrix. Along the diagonal, it accounts for the classical self
 83 radiation impedance of each aperture, and for the mutual radiation impedance between two
 84 apertures, it is assumed that they radiate as a monopole in an half infinite space.^{8,10,11} The
 85 input impedance is calculated from the knowledge of the quantities P_1 and U_1 .

86 At low frequencies the monopoles can be assumed to radiate into a full space, however, the
 87 uncertainty of the mutual loading approximation is greater than the factor of two between
 88 half space and full space radiation.

89 The TMMI impedance calculation yields subtly different results when compared with
 90 that of the standard TMM, as seen in Fig. 4. The two methods are in good agreement at
 91 low frequencies. At higher frequencies, the TMMI reduces the height of the resonances and
 92 reduces the depth of the anti-resonances, which can be interpreted as a reduction in the
 93 standing wave ratio of the resonator and an increase of the radiation losses in the system.
 94 Knowing P and U at the location of the toneholes allows for the calculation of external
 95 values such as directivity and the pressure waveform at a given external location, topics
 96 that are outside the scope of this paper but useful for future work.

97 III. RESONATOR DESIGN

98 A. Periodic lattice of holes and resulting cutoff frequency

99 The basic resonator considered in the current work is designed to have a desired first
 100 impedance resonance frequency at f_1 and desired cutoff frequency at f_c that can be ma-
 101 nipulated independently from one another by varying the geometry. This is achieved by
 102 concatenating a cylinder of length L , which largely determines f_1 , to a lattice of geometri-
 103 cally regular toneholes that imposes the cutoff behavior at f_c , as shown in Fig. 1(b). This
 104 is similar to the resonator design in the dissertation by Worman.¹² While not explained in
 105 great detail, it is important to note that simple geometric calculations must include low
 106 frequency length corrections, defined in Section III B, due to the lattice of toneholes as well
 107 as the more familiar radiation length correction at each open tonehole.

108 The analytic formulations used in this method allow only for the frequencies f_1 and f_c
 109 to be independently determined (see Eq. (2) and (4)). The second impedance peak of
 110 two resonators with different cutoff frequencies occur at nearly the same frequency because
 111 there is very low inharmonicity due to the cylindrical portion of the resonator, and the use
 112 of identical toneholes. Dimensions and acoustic features of sample resonators are provided
 113 in Appendix A.

115 B. Geometrically regular lattice

116 A geometrically (and therefore also acoustically) regular lattice is constructed by repeat-
 117 ing the basic cell shown in Fig. 1 (b) to create the lattice shown in Fig. 1 (a). If the cells are

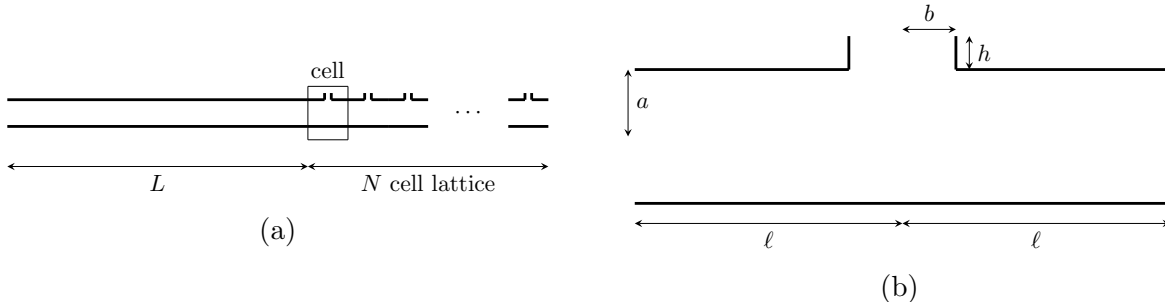


FIG. 1. Pipe and lattice resonator (a) constructed from identical cells (b).

118 all identical and their number infinite, the global cutoff frequency, which can be estimated
 119 from impedance measurements or simulations, will be equal to the local cutoff frequency.
 120 The local cutoff frequency is approximated by the Helmholtz resonance of a single cell whose
 121 main bore is closed at the extremities,¹³

$$\omega_c = 2\pi f_c \approx \frac{c}{\ell} \frac{1}{\sqrt{\left(\frac{c}{\ell}\right)^2 m_h C_a + 1/3}}, \quad (2)$$

122 where $C_a = 2\ell\pi a^2/\rho c^2$ is the acoustic compliance of the main pipe, $m_h = \rho h/\pi b^2$ is the
 123 acoustic mass of the tonehole, and a, ℓ, b and h are the geometric dimensions of the cell
 124 shown in Fig. 1 (b).

125 The exact local cutoff frequency for a cell in an infinite lattice can be calculated from

$$\frac{\ell}{c} \cot(k\ell) = \omega m_h C_a, \quad (3)$$

126 which is derived by solving the pressure and flow transfer matrix equations assuming either
 127 Dirichlet or Neumann boundary conditions within the main bore.⁹ This exact form differs
 128 by less than 1% from the approximate form given in Eq. (2) for an equivalent Helmholtz
 129 resonator of dimensions used in the current article. To impose a desired local cutoff frequency
 130 it is sufficient to find a combination of dimensions a, ℓ, b , and h , accounting for the length

131 corrections due to the inertial effect of adjacent fluid and the radiation impedance of the
 132 tonehole, that result in the desired resonance. Therefore, it is possible to design a lattice
 133 to have a desired global cutoff frequency by manipulating the dimensions of the constituent
 134 cells to have the same local cutoff frequency. To impose the frequency of the first impedance
 135 peak f_1 , a cylinder of length L is concatenated to the lattice and treated like a quarter-wave
 136 resonator,

$$f_1 = \frac{c}{4L_a}, \quad (4)$$

137 where $L_a = L + \Delta\ell$ is an effective acoustic length that accounts for the presence of a lattice of
 138 open toneholes. The lattice modifies the radiation impedance of the cylinder as a mass-like
 139 term, and is treated as a length correction

$$\Delta\ell = \ell\sqrt{1 + \frac{\ell^2}{c^2}C_a m_h}, \quad (5)$$

140 which must be included in addition to the physical length of the main cylinder when de-
 141 termining the appropriate length that results in the desired frequency f_1 .¹ A strong cutoff
 142 frequency behavior is observed with as few as three open toneholes, however, the frequency
 143 at which cutoff occurs tends to be somewhat higher than that calculated in Eq. (2) when
 144 the lattice is comprised of a small number of holes, see Fig. 2. Lattices with 10 toneholes
 145 exhibit a very strong cutoff behavior at the desired frequency. Three resonators, all with
 146 first resonance frequencies $f_1 = 170$ Hz and with cutoff frequencies $f_c = 1000, 1500,$ and
 147 2000 Hz, are used frequently in the current paper and will therefore be referred to as res-
 148 onators $\mathcal{R}_{1,0}$, $\mathcal{R}_{1,5}$ and $\mathcal{R}_{2,0}$. All three have ten toneholes in addition to the open termination
 149 of the pipe. The input impedance of all three were simulated and two ($\mathcal{R}_{1,0}$, $\mathcal{R}_{2,0}$) were

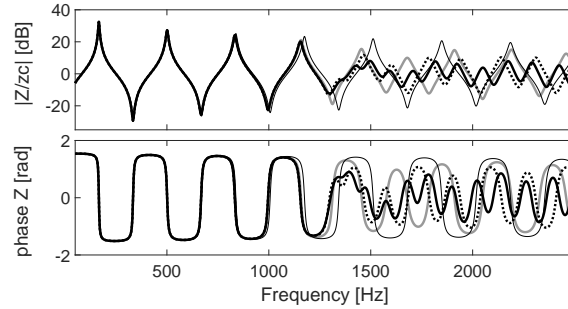


FIG. 2. Simulated impedance curves of resonators with $f_1 = 170$ Hz, $f_c = 1350$ Hz, and varying number of toneholes (thin solid black: cylinder; thick solid grey: 4 holes; thick dashed black: 10 holes; thick solid black: 20 holes). The cutoff frequency $f_c = 1350$ Hz was chosen to occur at an impedance minimum so that the effect on the next maximum can be more easily distinguished. Lattices with 10 holes exhibit very strong cutoff behavior.

150 constructed physically (dimensions provided in Appendix A) and compared with simulation
 152 in Section III D.

153 C. Acoustic regularity

154 Although the analysis based on digital synthesis in Section IV A is limited to a tone-
 155 hole network composed of geometrically regular cells, Moers and Kergomard¹³ show that
 156 it is possible to define an acoustic regularity for which each constituent cell has the same
 157 Helmholtz resonance, but not necessarily the same geometry. In that article, they consider
 158 the inverse problem of determining the division of an acoustically regular lattice that re-
 159 sults in the expected global cutoff frequency. In the present paper, the problem is solved
 160 directly by designing each cell to be geometrically different, except the bore radius, but have
 161 a common Helmholtz resonance, and therefore have an acoustic regularity that results in the

162 desired global cutoff frequency. The individual cells have identical main bore internal radii
 163 a , and the tonehole radii and heights b , h taken from the clarinet dimensions provided in
 164 Appendix A1 of Moers and Kergomard.¹³ Once a desired cutoff frequency is set, the length
 165 of pipe ℓ on each side of the symmetric cells is deduced by Eq. (2). This acoustically regular
 166 lattice can then be constructed with a leading pipe to create the desired first resonance peak
 167 described in Section III B. Figure 3 shows that a global cutoff frequency is attained using an
 168 acoustically (but not geometrically) regular lattice. As with a geometrically regular lattice,
 169 the low frequency behavior of the acoustically regular lattice is largely unchanged between
 170 resonators with different cutoff frequencies. Specifically, the height and frequency of the
 171 first two impedance peaks are negligibly different for different resonators. This similarity
 172 between geometrically and acoustically regular resonators suggests that the choice to use ge-
 173 ometrically regular resonators in this work is a reasonable simplification of real instruments,
 174 which exhibit substantial acoustic regularity. Next, the effect of the order of acoustically
 175 regular cells is examined by calculating the input impedance for randomized permutations
 176 of the cell locations. Figure 3 demonstrates that the order of the cells in the lattice does
 177 not greatly influence the frequency at which cutoff occurs and, as above, has a negligible
 178 influence on the height and frequency of the first two impedance peaks. This is a result
 179 of work by Fürstenberg¹⁴ demonstrating exceptions to the nonexistence of pass bands in
 180 an infinite one-dimensional random medium.^{13,15} It is worth noting that, above the cutoff
 181 frequency and up to approximately 2000 Hz, the impedance of each resonator, regardless of
 182 the cell order, follows similar and slowly diverging paths. This is unexpected and suggests
 183 that, for frequencies just above cutoff, the input impedance behavior is determined by global

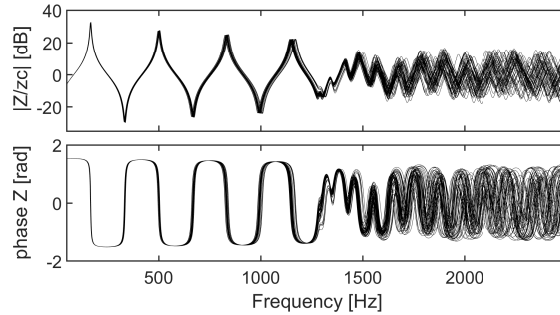


FIG. 3. Multiple simulated input impedances for resonators with acoustically regular lattices and random cell orders (50 permutations). The target frequencies are $f_1 = 170$ Hz and $f_c = 1350$ Hz.

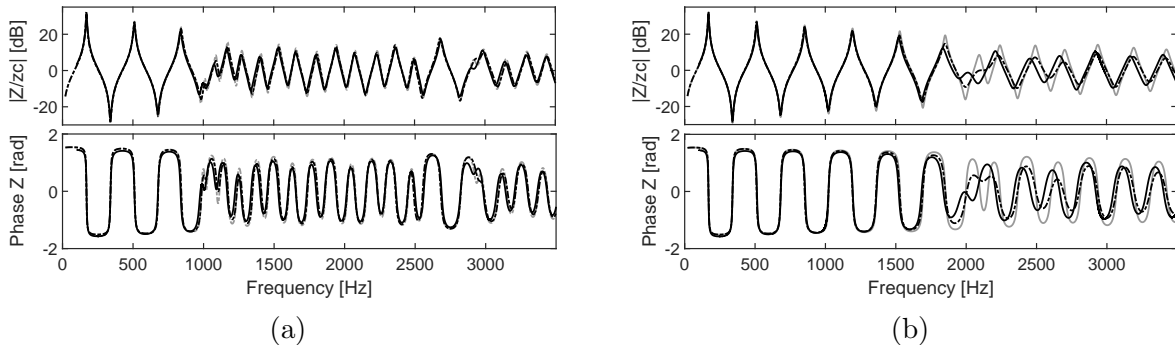


FIG. 4. Input impedance of $\mathcal{R}_{1,0}$ (a) and $\mathcal{R}_{2,0}$ (b). Grey: TMM simulation; dashed black: TMMI simulation; solid black: experimental.

184 features of the lattice. This is curious, but less relevant to the case of real clarinets, which
 185 typically have a fairly regular progression from small, closely spaced holes near the top of
 186 the instrument, to large and distantly spaced holes near the bell.

188 **D. Experimental results of a simple resonator**

189 The simplified pipe-lattice resonator described in the previous section was tested experi-
 190 mentally by measuring the input impedance of two polyamide 6 tubes where the lengths L

191 and tonehole network geometries are designed to have first impedance resonances at 170 Hz
 192 and cutoff frequencies at 1000 Hz and 2000 Hz ($\mathcal{R}_{1,0}$, $\mathcal{R}_{2,0}$), according to Eq. (2) and (4).
 193 The dimensions are summarized in Appendix A. The input impedance was measured using
 194 an impedance measurement device developed at CTTM.¹⁶ Figure 4 shows that the target
 195 first impedance resonance and cutoff frequencies are attained by both simulation and mea-
 196 surements. This demonstrates the relevance of the model and accuracy of the measurement
 197 methodology. The better agreement between simulation and measurement for the $f_c = 1000$
 198 Hz resonator is a consequence of the greater distance between holes, and not a general trend
 199 related to the cutoff frequency of a resonator. A second stop band in the impedance of $\mathcal{R}_{1,0}$ is
 200 visible around 2500 Hz both in the simulation and measurement. The discrepancy between
 201 simulation and measurements at high frequencies may be due to slight imprecision of the
 202 physical geometries of the experimental pipes, inaccuracies of the measurement hardware,
 203 or higher order phenomena not included in the simulation. These differences do not affect
 204 the conclusions, which are based on the location of the cutoff frequency and not the precise
 205 high frequency behavior.

206 IV. EFFECTS OF CUTOFF FREQUENCY USING DIGITAL SYNTHESIS

207 Digital sound synthesis is a convenient method to evaluate the playing characteristics of
 208 a real or hypothetical resonator, and to compare two or more different resonators, because
 209 it can synthesize time domain acoustic pressure and volume velocity waveforms inside the
 210 mouthpiece for a wide range of control parameters. One can then compute descriptors of
 211 the waveform that are used to quantify playing characteristics, with respect to the control

212 parameters, such as playing frequency, spectral centroid, and attack time. These playing
 213 descriptors are functions of the dimensionless control parameters excitation pressure γ , and
 214 embouchure ζ (defined below), but also are dependent on the reed parameters and input
 215 impedance of the resonator.^{17,18} It is assumed that γ and ζ control timbre features of a given
 216 instrument, and are therefore useful parameters to evaluate the connection between sound
 217 production and sound descriptors. It is important to note that synthesized waveforms do
 218 not necessarily match those of a real instrument because the values of physical parameters,
 219 particularly regarding the reed dynamics, are not precisely known. However, digital synthesis
 220 is a reasonable tool to compare the behavior of different resonators. The following sections
 221 are based on synthesis for resonators $\mathcal{R}_{1.0}$, $\mathcal{R}_{1.5}$ and $\mathcal{R}_{2.0}$ as defined in Section III B.

222 A. Digital synthesis model

223 The digital synthesis model used in this work combines the discretization scheme
 224 of Guillemain,¹⁷ with the use of the reflection function to model the response of the
 225 resonator.^{19,20} Its purpose is to solve, in the domain of time sampled signals, a system
 226 of three equations and three unknowns giving the values at sample number n as functions of
 227 the past known values of the three variables. For that purpose, we start with the continuous
 228 time model describing the resonator, the reed dynamics, and the nonlinear relationship
 229 between pressure and flow in the mouthpiece.

1. Continuous time model

The continuous time reed instrument model used in this work is comprised of three main equations (Eq. (7), (9), and (10)). The three variables are the dimensionless pressure, flow rate, and reed displacement, respectively

$$\begin{cases} \tilde{p}(t) = p(t)/p_M \\ \tilde{u}(t) = Z_c u(t)/p_M, \\ \tilde{x}(t) = x(t)/H, \end{cases} \quad (6)$$

where Z_c is the characteristic impedance, p_M is the pressure difference needed to close the reed completely in a static situation, and H is the distance between the tip of the reed and the mouthpiece lay at equilibrium. The value $\tilde{x} = -1$ corresponds to the closure of the reed. The first equation corresponds to the movement of the reed which consists of a damped spring-mass driven by the pressure differential between the mouth of the musician and the mouthpiece

$$\begin{cases} \frac{1}{\omega_r^2} \frac{d^2 \tilde{x}(t)}{dt^2} + \frac{q_r}{\omega_r} \frac{d\tilde{x}(t)}{dt} + \tilde{x}(t) = \tilde{p}(t) - \gamma \text{ if } \tilde{x} > -1, \\ \frac{d\tilde{x}(t)}{dt} = 0 \text{ if } \tilde{x} < -1, \end{cases} \quad (7)$$

where ω_r is the resonance angular frequency of the reed, q_r is the damping coefficient, and the parameter $\gamma = p_m/p_M$ is the dimensionless pressure in the mouth of the musician. Following values similar to other articles,¹⁸ the synthesis results presented in this paper assume $\omega_r = 2\pi f_r = 2\pi 1500$ (rad/s) and $q_r = 0.4$ (dimensionless). The second line of Eq. (7) corresponds to the limitation of the reed displacement by the mouthpiece lay. There exist more refined models of the reed that include dynamical behavior and the collision of the reed

and the lay.^{22–24} These models, however, are unnecessary for the current work which aims to efficiently compare the response of different resonators, not predict absolute behavior. The nonlinear relationship relating the input flow $u(t)$ as a function of the pressure differential and the reed position is

$$\tilde{u}(t) = u_b(t) + u_r(t), \quad (8)$$

where

$$\begin{cases} u_b(t) = \zeta(1 + x(t))\text{sign}(\gamma - \tilde{p}(t))\sqrt{|\gamma - \tilde{p}(t)|}, \\ u_r(t) = \lambda_c \frac{dx(t)}{dt}. \end{cases} \quad (9)$$

²³¹ The variable $\zeta = Z_c w H \sqrt{2/\rho p_M}$ is the dimensionless embouchure parameter, depending on
²³² the width w and height H of the reed channel cross section when the reed is at rest, and is
²³³ proportional to the square root of H because p_M is a function of H . The total flow rate is
²³⁴ the sum of the flow computed from the stationary Bernoulli equation u_b and the flow due to
²³⁵ the movement of the reed u_r , depending on the speed of the reed and a parameter λ_c that
²³⁶ characterizes the effective vibrating surface of the reed.²⁵

The third principle equation represents the passive role of the resonator and is expressed by its input impedance. Following McIntyre²⁶ and Gazengel,¹⁹ a straightforward change of variables in the Fourier domain, using wave variables rather than Kirchhoff variables, leads to the expression of the backward pressure wave at time t in the temporal domain

$$p^-(t) = (r * p^+)(t), \quad (10)$$

237 where $p^-(t) = (\tilde{p}(t) - \tilde{u}(t))/2$ and $p^+(t) = (\tilde{p}(t) + \tilde{u}(t))/2$ are the backward and forward
 238 pressure waves in the resonator. The operator $*$ represents continuous time convolution and
 239 r is the reflection function of the resonator, obtained from the input impedance by

$$r = \mathcal{F}^{-1} \left(\frac{Z(\omega) - Z_c}{Z(\omega) + Z_c} \right), \quad (11)$$

240 where \mathcal{F}^{-1} is the inverse Fourier transform. The advantage of using the reflection function
 241 rather than the impulse response is that it is assumed to decrease much faster in time, and
 242 can therefore be truncated to save computation time.

243 *2. Discrete model*

244 The continuous time model of the complete instrument is discretized so that temporal
 245 synthesis can be simulated by a computer. Therefore, a strictly causal formulation must
 246 be found so that every variable at a given time sample can be computed from the previous
 247 values of all variables. Equation (7) is discretized using the finite difference scheme,²⁰ such
 248 that

$$x[n] = b_{1r}p[n-1] + a_{1r}x[n-1] + a_{2r}x[n-2], \quad (12)$$

249 where the tilde notation is omitted for dimensionless variables in the discrete formulation
 250 ($p[n]$ is the n^{th} sample of the dimensionless pressure signal). The coefficients b_{1r} , a_{1r} and a_{2r}
 251 are given in Guillemain et al.²⁰ In order to ensure the limitation of the reed displacement,
 252 the following condition is added

$$\text{if } x[n] < -1, \text{ then } x[n] = x[n - 1]. \quad (13)$$

253 Once the position of the reed at sample n is known, the reed flow is computed using the
 254 finite difference scheme

$$u_r[n] = \lambda(x[n] - x[n - 1]). \quad (14)$$

The parameter $\lambda = \lambda_c f_s$ is fixed at the value -0.7 as in Coyle et al.¹⁸ based on the measurements available in the literature.²⁵⁻²⁸ The third equation involving the reflection function can be reformulated using the discrete convolution product

$$(r * p^+)[n] = \sum_{i=0}^{\infty} r[i]p^+[n - i], \quad (15)$$

where r is the discrete version of the reflection function, which is causal. For the numerical application, the reflection function is deduced from the computed input impedance, which is windowed down to the characteristic impedance by 8 kHz, well below the first nonplanar mode and following recommendations from Gazengel.¹⁹ Above this frequency the impedance is completed by the characteristic impedance until the Nyquist frequency, before computing the reflection function by inverse Fourier transform. Only the first $D = 3000$ elements of the reflection function are kept for the synthesis, chosen to be long enough so that it does not disturb the low frequency content of the resonator's response. Specifically, the impulse response is a sum of exponentially damped sinusoids and this choice of D ensures that the time response of the lower mode, with the highest quality factor, is not truncated. The

backward pressure wave corresponds is written as

$$p^-[n] = \sum_{i=0}^D r[i]p^+[n-i]. \quad (16)$$

Separating this equation into a strictly causal and an instantaneous part and substituting for p and u , $p^-[n]$ becomes

$$\frac{1}{2}(p[n] - u[n]) = \frac{1}{2}r[0](p[n] + u[n]) + \frac{1}{2}\sum_{i=1}^D r[i](p[n-i] + u[n-i]), \quad (17)$$

where $r[0]$ is the first sample of the discrete reflection function. This yields $p[n]$ as a function of $u[n]$ and the past of p and u

$$p[n](1 - r[0]) = u[n](1 + r[0]) + \sum_{i=1}^D r[i](p[n-i] + u[n-i]), \quad (18)$$

The final pressure expression is as follows:

$$p[n] = \frac{1 + r[0]}{1 - r[0]}u[n] + \frac{1}{1 - r[0]}\sum_{i=1}^D r[i](p[n-i] + u[n-i]). \quad (19)$$

255 Using Eq. (19), it is possible to implement the temporal synthesis scheme described in
 256 Guillemain et al.,²⁰ because it is in the form $p[n] = b_{c_o}u[n] + V$ where V is a known quantity
 257 at sample n .

258 B. Results

259 Synthesized time and frequency domain waveforms of the internal pressure and flow for
 260 resonators $\mathcal{R}_{1.0}$, $\mathcal{R}_{1.5}$, and $\mathcal{R}_{2.0}$ are shown in Fig. 5, and available to listen to online²¹. The
 261 waveforms are taken from the periodic and steady state region of the synthesis, which is
 262 calculated with control parameters $\gamma = 0.45$, $\zeta = 0.45$. In this representation the signals

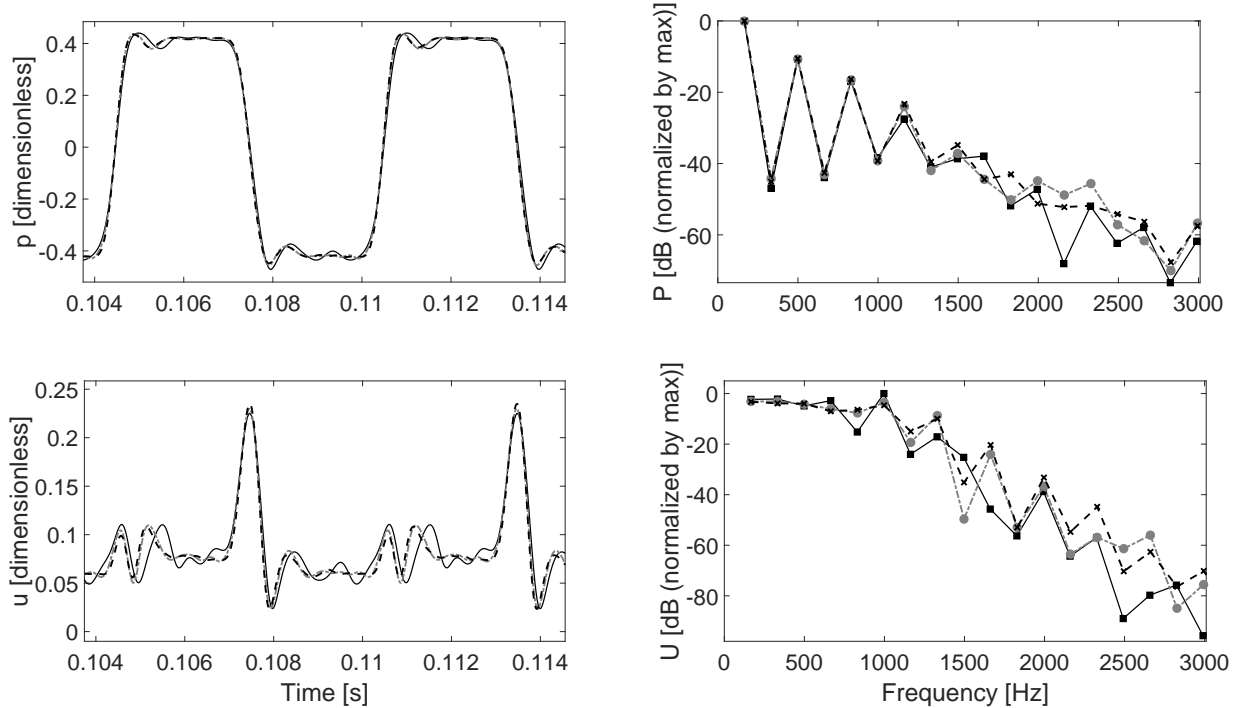


FIG. 5. Synthesized (dimensionless) pressure (top) and flow (bottom) inside mouthpiece for resonators $\mathcal{R}_{1.0}$ (solid black), $\mathcal{R}_{1.5}$ (dash-dot gray), and $\mathcal{R}_{2.0}$ (dashed black) in the time (left) and frequency (right) domains. Control parameters are $\gamma = \zeta = 0.45$, and reed resonance $f_r = 1500$ Hz.

263 from the three resonators have been arbitrarily shifted in time by less than one cycle, so
 264 that they overlay one another, facilitating visual comparison. The timing difference of the
 265 pressure and flow signals is small, and may result from a small change in playing frequency.
 266 There is a subtle difference between both the pressure and volume velocity for resonators
 267 $\mathcal{R}_{1.0}$, $\mathcal{R}_{1.5}$, and $\mathcal{R}_{2.0}$. The biggest visual difference is in the volume velocity waveform, in
 268 which resonator $\mathcal{R}_{1.0}$ has larger amplitude and lower frequency rippling when compared
 269 with resonators $\mathcal{R}_{1.5}$ and $\mathcal{R}_{2.0}$. A simple interpretation, examined in Section IV B 1, is that
 270 there is more energy in the high frequency harmonics in the waveforms computed from
 271 resonators with higher cutoff frequencies. The height of the peaks that are the main feature

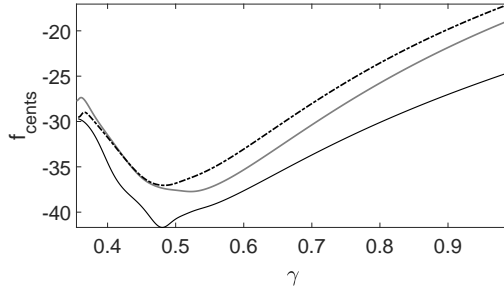


FIG. 6. Synthesized playing frequency in cents, normalized by the first impedance peak frequency, for resonators $\mathcal{R}_{1.0}$, $\mathcal{R}_{1.5}$, and $\mathcal{R}_{2.0}$ with solid black, solid grey, dashed black lines, respectively.

272 in the velocity waveform, corresponding to the closing of the reed, also changes between the
 273 different resonators.

274 1. Frequency domain characteristics

275 Frequency domain characteristics are computed directly from the steady state portion of
 276 the synthesized waveforms p and u inside the mouthpiece, discarding the attack transient.
 277 The playing frequency, f_p , of resonators $\mathcal{R}_{1.0}$, $\mathcal{R}_{1.5}$, and $\mathcal{R}_{2.0}$, as a function of γ with constant
 278 $\zeta = 0.45$, are displayed in Fig. 6. The values are presented in cents, relative to the frequency
 279 of the first impedance peak, such that

$$f_{\text{cents}} = 1200 \log_2 \left(\frac{f_p}{f_1} \right). \quad (20)$$

280 It is seen that resonators with higher cutoff frequencies also have playing frequencies that
 281 are higher by a few cents. In the beating reed regime, approximately $\gamma > 0.5$, the difference
 282 between resonators $\mathcal{R}_{1.0}$ and $\mathcal{R}_{2.0}$ is greater than five cents, therefore possible large enough
 283 to be perceived by a human.²⁹ This is not due only to the difference in inharmonicity
 284 between the first and second peaks, verified through analytical formulations,¹⁸ in which

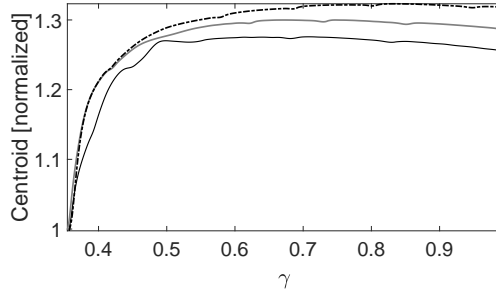


FIG. 7. Synthesized spectral centroid, normalized by the playing frequency, for resonators $\mathcal{R}_{1.0}$, $\mathcal{R}_{1.5}$, and $\mathcal{R}_{2.0}$ with solid black, solid grey, dashed black lines, respectively.

285 the inharmonicity of these resonators results in a maximum of 2.5 cents difference between
 286 resonators $\mathcal{R}_{1.0}$ and $\mathcal{R}_{2.0}$. However, the tonehole lattice also changes the inharmonicity of
 287 higher resonances of the input impedance below the cutoff frequency. This could influence
 288 the playing frequency, particularly at high values of γ and ζ .

289 To define a single value descriptor, the spectral centroid³⁰ is calculated as

$$\text{centroid} = \frac{\sum_{m=1}^M f(m)G(m)}{\sum_{m=1}^M G(m)}, \quad (21)$$

290 where $G(m)$ is the single sided power spectrum corresponding to the Fast Fourier Transform
 291 frequency bins $f(m)$ up to $f(M) = 8$ kHz, at which point the assumptions made in the
 292 impedance simulation regarding thermo-viscous losses and radiation are no longer valid.
 293 This definition results in a single number for a given spectrum with units of Hz, which
 294 follows the ‘center of mass’ interpretation of the spectral content. The spectral centroid
 295 values, normalized by the playing frequency at each combination of control parameter and
 296 for each resonator, are shown in Fig. 7. The spectral centroid is higher for resonators with
 297 higher cutoff frequencies, even after adjusting for the playing frequency.

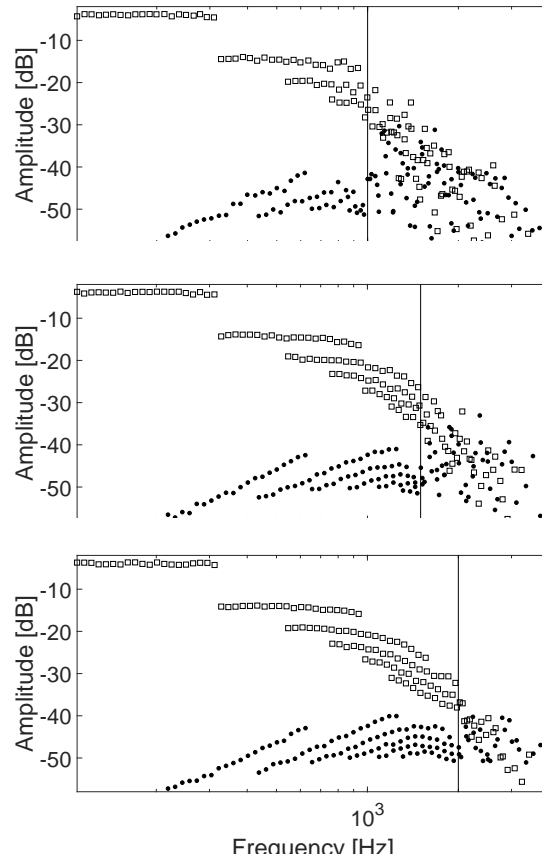


FIG. 8. Synthesized ($\zeta = 0.45$, $\gamma = 0.55$) spectra of the mouthpiece pressure for resonators $\mathcal{R}_{1.0}$, $\mathcal{R}_{1.5}$, and $\mathcal{R}_{2.0}$ for 20 fundamental frequencies ranging chromatically from 110 Hz to 330 Hz. Odd and even harmonics denoted by squares and circles, respectively.

299 To evaluate the influence on the distribution of harmonics in synthesized signals, the
 300 input impedance was simulated for a wide range of resonators with fundamental frequencies
 301 of 20 consecutive semitones ranging from 110 to 330 Hz for all three cutoff frequencies 1000,
 302 1500, and 2000 Hz. This results in 60 simulated resonators: 20 of each type $\mathcal{R}_{1.0}$, $\mathcal{R}_{1.5}$ and
 303 $\mathcal{R}_{2.0}$. The first impedance peak frequency is manipulated by changing the length of the
 304 cylinder between the mouthpiece and the first open tonehole, leaving the lattice of 10 open
 305 toneholes unchanged. Digital sound synthesis was then calculated for the 60 resonators,

306 using a beating regime value $\zeta = 0.45$, $\gamma = 0.55$ in order to generate more even harmonics.
 307 A peak detection scheme was applied to the spectra of the internal pressure where the square
 308 and circular data markers correspond to the odd and even harmonics. The results are plotted
 309 in Fig. 8 for resonators of type $\mathcal{R}_{1.0}$, $\mathcal{R}_{1.5}$ and $\mathcal{R}_{2.0}$ in top, middle, and bottom, respectively,
 310 and vertical lines denote the cutoff frequency of the resonators used in each figure.

311 For all resonators shown here, regardless of their cutoff frequency, the odd harmonics
 312 that are below the cutoff frequency have approximately the same amplitude climbing the
 313 semitone scale. Around and above the cutoff frequency the amplitudes of the odd harmonics
 314 decreases, and the strong organization disappears as also seen in Fig. 5, which implies that
 315 the complicated input impedance above cutoff frequency has a randomizing effect on the
 316 production of odd harmonics. This can be interpreted as the system no longer behaving as
 317 a quarter-wave resonator at these frequencies. Additionally, the even harmonics generally
 318 grow in amplitude as a function of frequency, and display a marked increase in amplitude for
 319 frequencies higher than the cutoff frequency. This implies that below the cutoff frequency,
 320 the spectral content of the waveforms produced by resonators with different cutoff frequencies
 321 is relatively similar, but that the high frequency spectra, and hence the perceived sound,
 322 can be quite different above the cutoff frequency. Specifically, the plots show more energy
 323 in even harmonics above the cutoff frequency.

The same 60 resonators are compared in terms of the time averaged intensity at input
 of the resonators and the the time averaged intensity summed over each radiating aperture,

shown in Fig. 9. The time averaged intensity is defined as

$$\langle I_{\text{in}} \rangle = \frac{1}{2} \text{Re}[P_0 U_0^*], \quad (22)$$

$$\langle I_{\text{rad}} \rangle = \sum_{n=1}^M \frac{1}{2} \text{Re}[P_n U_n^*], \quad (23)$$

324 where $M = N + 1$ is the number of toneholes N plus the open end of the resonator. This
 325 provides a direct comparison between the energy that remains inside the resonator and con-
 326 tributes to the auto-oscillation and the total energy that exits the resonator. A comparison
 327 of the left and right panels shows that the time averaged intensity of the fundamental fre-
 328 quency at the input is on the order of 40 dB higher than the output, suggesting that the
 329 resonators are inefficient sound sources, regardless of cutoff frequency. Note that the level
 330 of the fundamental frequency input intensity is not horizontal as it is for pressure in the
 331 mouthpiece. The output intensity of the fundamental frequency increases proportional to
 332 ω^2 . This is consistent with known monopole radiation efficiency and bolsters the claim that,
 333 below the cutoff frequency, the main radiating source can be treated as a monopole at the
 334 location of the first open tonehole. Above the cutoff frequency the time averaged intensity
 335 is approximately the same for the input and output. This implies that the resonators are
 336 more efficient sources above the cutoff frequency.

337 It is concluded that the cutoff frequency affects the spectral content of waveforms within
 338 the mouthpiece by both demarcating the frequency at which even harmonics develop, as
 339 well as shifting the spectral centroid higher for resonators with higher cutoff frequencies.

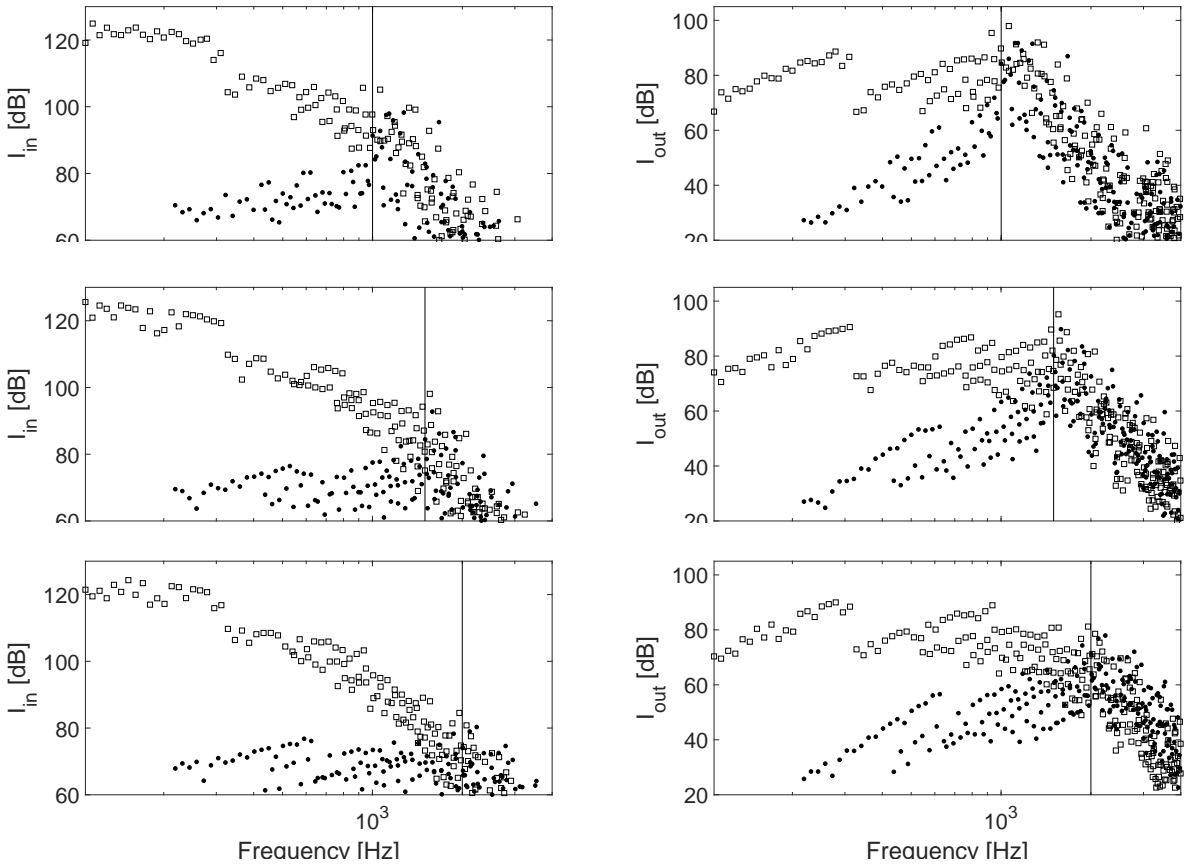


FIG. 9. Time averaged intensity passing through the entrance of the resonator (left) and the summed over ten toneholes and exit of resonator (right). Resonators and synthesis control parameters are the same as in Fig 8. The cutoff frequency for each set of resonators is marked by a vertical line.

340 2. Attack time

341 To evaluate the influence of the cutoff frequency on the transient portion of the wave-
 342 form, the time evolution of the waveform as the musician increases the blowing pressure
 343 from atmospheric pressure ($\gamma = 0$) to the steady state value of γ is simulated. To avoid
 344 discontinuities in the onset pressure, the transition from $\gamma = 0$ to the steady state value

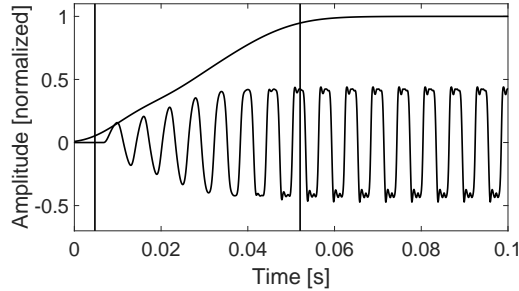


FIG. 10. Synthesized pressure waveform and sum of time evolving harmonics for resonator $\mathcal{R}_{1.0}$ with 5% and 95% thresholds marked.

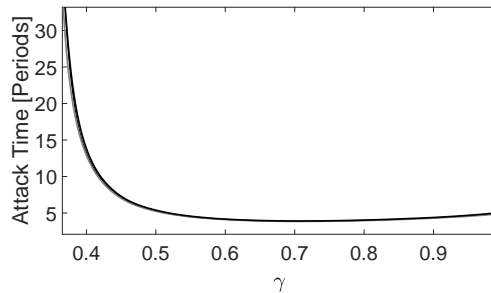


FIG. 11. Synthesized attack time normalized by period of playing frequency for resonators $\mathcal{R}_{1.0}$, $\mathcal{R}_{1.5}$ and $\mathcal{R}_{2.0}$ with solid black, solid grey, dashed black lines, respectively. Variation in attack times due to cutoff frequency is generally less than 10%.

345 follows the curve of the first half of a Hann window. In the current work the duration of
 346 the transition is 201 samples, corresponding to about five milliseconds for a sampling rate
 347 of 44100 samples per second. To define the attack time, the time domain pressure signal is
 348 decomposed into its constituent harmonics, each of which evolves as a function of time. To
 349 include frequencies above the cutoff frequency of all resonators, 16 harmonics are considered.
 350 The harmonics are calculated by an inverse Fourier transform on windowed versions of the
 351 spectrum around each harmonic. This estimates the instantaneous amplitude and frequency

352 of each harmonic for the duration of the signal, including during the attack transient. The
 353 sum of the squared amplitude of these bands is proportional to the total energy in the signal
 354 at a given instant, and the energy in the steady state portion of the signal can be determined
 355 by choosing this value well into the steady state portion of the signal. The beginning of
 356 the attack is determined when the signal first passes a threshold that is a specific, arbitrary
 357 fraction of the final value, and the end of the signal attack is defined as the last time that the
 358 sum is outside a threshold from the steady state value. Onset threshold values of 5 and 10
 359 percent, and ending threshold values of 90 and 95 percent have been investigated. Figure 10
 360 shows a typical pressure waveform onset (in this case for $\mathcal{R}_{1.0}$), with the sum of the first 16
 361 harmonics, normalized to have a maximum value of unity, superimposed. The threshold at
 362 5% and 95% are marked in bold lines. It is found in this work that the attack time is linearly
 363 related to the choice of threshold, and therefore any of these four choices (5-90, 5-95, 10-90,
 364 10-95) is reasonable for comparing the attack time of different resonators. Figure 11 shows
 365 the attack time normalized by the period of the playing frequency as a function of γ with
 366 constant $\zeta = 0.45$. Thresholds of 5% and 95% are used to define the onset and saturation
 367 of the waveform. The attack time of resonators $\mathcal{R}_{1.0}$, $\mathcal{R}_{1.5}$, and $\mathcal{R}_{2.0}$ are sufficiently similar
 368 as to be difficult to discern. The difference between attack times of different resonators is
 369 less than 10% of a period for $\gamma > 0.5$, and up to 2.5 periods for $\gamma < 0.5$. However, for low
 370 blowing pressures the attack time is of the order of tens of periods, so the difference of 2.5
 371 periods is still a small percentage of the total attack time. It is concluded that the cutoff
 372 frequency does not strongly impact the attack time of a given resonator which, in a musical
 373 context, may be related to the ease of playing.

374 **V. CONCLUSION**

375 The acoustic resonators developed in this work are adapted for studying the effect of
376 the cutoff frequency on sound production and, potentially, radiation. The simple nature
377 of these resonators, for which it is possible to independently vary the frequencies of both
378 the first impedance peak and the cutoff frequency, is particularly useful because the low
379 frequency behavior (below cutoff) is largely the same for resonators with very different high
380 frequency behavior. The data resulting from either digital sound synthesis or experimental
381 measurements can then be used to directly assess the effect of the cutoff frequency on the
382 sound production and resulting external sound field.

383 It is found that the cutoff frequency does affect the synthesized waveform within the
384 mouthpiece, particularly the spectral characteristics. Resonators with a higher cutoff fre-
385 quency have higher playing frequencies, and higher spectral centroids, when compared with
386 resonators with lower cutoff frequencies. Furthermore, even harmonics tend to be excited
387 above the cutoff frequency of a given resonator. However, the differences between internal
388 waveforms in resonators with different cutoff frequencies is subtle. Furthermore, the cutoff
389 frequency of a resonator is not found to have a significant influence on the attack time,
390 showing that one measure of the “playability” of a clarinet-like instrument relies more on
391 the low frequency response of the resonator. This implies that an instrument maker may
392 be able to make modifications to the geometry of an instrument that results in a different
393 cutoff frequency, without the risk of greatly changing the sound production qualities of the
394 instrument.

395 In contrast to the relatively small effect of the cutoff frequency on sound production,
396 the cutoff frequency has a larger impact on the high frequency spectral characteristics and
397 radiation. The radiation efficiency, calculated as the ratio of the time averaged intensity at
398 the input of the instrument with that summed over the radiating apertures, is higher above
399 the cutoff frequency than below. Above the cutoff frequency the resonators produce more
400 even harmonics and radiate more efficiently, implying that the cutoff frequency could have
401 a substantial impact on the perceived timbre of different instruments, or different notes on
402 the same instrument.

403 This, along with the small impact on sound production, indicates that the cutoff frequency
404 may be used to change the timbre characteristics of an instrument without altering its sound
405 production qualities.

406 Future work includes extending the synthesis analysis to the external sound field to
407 evaluate the effect of the cutoff frequency on radiated sound, for which Fig. 9 provides an
408 initial answer. This includes directivity of the source due to multiple radiating apertures. A
409 characterization of the external sound field can then be compared with the internal sound
410 field to evaluate the competition between sound production and radiation of clarinet-like
411 musical instruments.

412 **ACKNOWLEDGMENTS**

413 This work has been partly supported by the french Agence Nationale de la Recherche
414 (ANR16-LCV2-0007-01 Liamfi project). The authors would also like to thank Patrick
415 Sanchez and Guy Rabau for their help with the impedance measurements.

TABLE I. Dimensions for two prototype resonators with the first impedance peak f_1 at 170 Hz and cutoff frequencies f_c at 1000 Hz and 2000 Hz. Simulated and measured input impedance are provided in Fig. 4.

Resonator	L [mm]	a [mm]	ℓ [mm]	b [mm]	h [mm]
$\mathcal{R}_{1,0}$	436.7	7.0	32.8	4.0	8.4
$\mathcal{R}_{2,0}$	470.1	7.0	8.9	4.0	8.4

416 APPENDIX A: MEASUREMENTS: PROCEDURE AND MATERIALS

417 Two resonators were realized to experimentally verify the feasibility of designing res-
 418 onators with independently chosen first input impedance peaks and cutoff frequencies. The
 419 resonators were made by drilling holes in polyamide 6 tubes, the dimensions of which are
 420 summarized in Table I. The input impedance was then measured using the impedance mea-
 421 surement device developed at CTTM in hemi-anechoic conditions.¹⁶ Table II summarizes
 422 the first two impedance peak frequencies of resonators $\mathcal{R}_{1,0}$, $\mathcal{R}_{1,5}$, and $\mathcal{R}_{2,0}$ used for the
 423 digital synthesis. The inharmonicity, in cents, is defined as

$$\text{inharmonicity} = 1200 \log_2 \left(\frac{f_2}{3f_1} \right). \quad (\text{A1})$$

TABLE II. Frequencies of the first two impedance peaks and inharmonicity of resonators $\mathcal{R}_{1.0}$, $\mathcal{R}_{1.5}$, and $\mathcal{R}_{2.0}$.

Resonator	f_c [Hz]	f_1 [Hz]	f_2 [Hz]	inharm [cents]
$\mathcal{R}_{1.0}$	1000	170	511.6	5.4
$\mathcal{R}_{1.5}$	1500	170	513.0	10.2
$\mathcal{R}_{2.0}$	2000	170	513.1	10.5

427 References

428 ¹A. H. Benade, *Fundamentals of Musical Acoustics* (Oxford University Press, London,
429 1976).

430 ²L. Brillouin and M. Parodi, *Wave propagation in periodic structures* (Mc Graw Hill, New
431 York, NY, USA, 1946).

432 ³A. H. Benade, “On the mathematical theory of woodwind finger holes,” *J. Acoust Soc.*
433 *Am.* **32**, 1591–1608 (1960).

434 ⁴J. Wolfe and J. Smith, “Cutoff frequencies and cross fingerings in baroque, classical, and
435 modern flutes,” *J. Acoust Soc. Am.* **114**(4), 2263–2272 (2003).

436 ⁵G. R. Plitnik and W. J. Strong, “Numerical method for calculating input impedances of
437 the oboe,” *J. Acoust Soc. Am.* **65**(3), 816–825 (1979).

438 ⁶R. Causse, J. Kergomard, and X. Lurton, “Input impedance of brass musical instruments—
439 comparison between experiment and numerical models,” *J. Acoust Soc. Am.* **75**(1), 241–

440 254 (1984).

441 ⁷D. Keefe, “Woodwind air column models,” *J. Acoust Soc. Am.* **88**, 35–51 (1990).

442 ⁸A. Lefebvre, G. P. Scavone, and J. Kergomard, “External tonehole interactions in wood-
443 wind instruments,” *Acta Acustica united with Acustica* **99**, 975–985 (2013).

444 ⁹A. Chaigne and J. Kergomard, *Acoustics of Musical Instruments* (Springer-Verlag, New
445 York, 2016), (English translation).

446 ¹⁰R. L. Pritchard, “Mutual acoustic impedance between radiators in an infinite rigid plane,”
447 *J. Acoust Soc. Am.* **32**(6), 730–737 (1960).

448 ¹¹P. Rucz, “A finite element approach for the calculation of self and mutual radiation
449 impedances of resonators,” *J. Acoust Soc. Am.* **143**(4), 2449–2459 (2018).

450 ¹²W. E. Worman, “Self-sustained nonlinear oscillations of medium amplitude in clarinet like
451 systems,” Ph.D. thesis, Case Western Reserve University, 1971.

452 ¹³E. Moers and J. Kergomard, “On the cutoff frequency of clarinet-like instruments. ge-
453 ometrical versus acoustical regularity,” *Acta Acustica united with Acustica* **97**, 984–96
454 (2011).

455 ¹⁴H. Fürstenberg, “Noncommuting random matrix products,” *Trans. Am. Math. Soc.* **108**,
456 377–428 (1963).

457 ¹⁵P. W. Anderson, “Absense of diffusion in certain random lattices,” *Phys. Rev.* **109**, 1492–
458 1505 (1958).

459 ¹⁶J. C. L. Roux, M. Parchebat, and J. Dalmont, “A new impedance sensor for industrial
460 applications,” *Conf. Proceedings: Acoustics 2012* (2012).

461 ¹⁷P. Guillemain, “A digital synthesis model of double-reed wind instruments,” EURASIP
462 Journal on Applied Signal Processing **7**, 990–1000 (2004).

463 ¹⁸W. L. Coyle, P. Guillemain, J. Kergomard, and J.-P. Dalmont, “Predicting playing frequen-
464 cies for clarinets: A comparison between numerical simulations and simplified analytical
465 formulas,” J. Acoust Soc. Am. **138**(5), 2770–2781 (2015).

466 ¹⁹B. Gazengel, J. Gilbert, and N. Amir., “Time domain simulation of single-reed wind
467 instrument. From the measured input impedance to the synthesis signal. Where are the
468 traps?,” Acta Acustica united with Acustica **3**, 445–472 (1995).

469 ²⁰P. Guillemain, J. Kergomard, and T. Voinier, “Real-time synthesis of clarinet-like instru-
470 ments using digital impedance models,” J. Acoust Soc. Am. **118**, 483–494 (2005).

471 ²¹E. Petersen, “[url will be inserted by aip],” Synthesized mouthpiece waveforms as audio for
472 pressure SuppPubmm1-3, acoustic flow SuppPubmm4-6, and time derivative of pressure
473 plus flow SuppPubmm7-9 (an approximation of raidated sound), for resonators with cutoff
474 frequencies of 1000, 1500, and 2000 Hz..

475 ²²F. Avanzini and M. Walstijn, “Modelling the mechanical resonance of the reed-mouthpiece-
476 lip system of a clarinet. part i. a one-dimensional distributed model,” Acta Acustica united
477 with Acustica **90**, 537–547 (2004).

478 ²³M. Walstijn and F. Avanzini, “Modelling the mechanical resonance of the reed-mouthpiece-
479 lip system of a clarinet. part ii: A lumped model approximation,” Acta Acustica united
480 with Acustica **93**, 435–446 (2007).

481 ²⁴S. Bilbao, A. Torin, and V. Chatziioannou, “Numerical modeling of collisions in musical
482 instruments,” *Acta Acustica united with Acustica* **101**, 155–173 (2015).

483 ²⁵J.-P. Dalmont, P. Guillemain, and P.-A. Taillard, “Influence of the reed flow on the into-
484 nation of the clarinet,” in *Acoustics 2012* (2012).

485 ²⁶M. E. McIntyre, R. T. Schumacher, and J. Woodhouse, “On the oscillations of musical
486 instruments,” *J. Acoust Soc. Am.* **74**, 1325–1345 (1983).

487 ²⁷J. P. Dalmont, B. Gazengal, J. Gilbert, and J. Kergomard, “Some aspects of tuning and
488 clean intonation in reed instruments,” *Applied Acoustics* **46**, 19–60 (1995).

489 ²⁸J. Dalmont, J. Joël, and S. Ollivier, “Nonlinear characteristics of single-reed instruments:
490 Quasistatic volume flow and reed opening measurements,” *J. Acoust Soc. Am.* **114**(4),
491 2253–2262 (2003).

492 ²⁹E. G. Shower and R. Biddulph, “Differential pitch sensitivity of the ear,” *J. Acoust Soc.*
493 *Am.* **3**, 275–287 (1931).

494 ³⁰S. McAdams, J. W. Beauchamp, and S. Meneguzzi, “Discrimination of musical instrument
495 sounds resynthesized with simplified spectrotemporal parameters,” *J. Acoust Soc. Am.*
496 **105**(2), 882–897 (1999).

497 List of Figures

498	1	Pipe and lattice resonator (a) constructed from identical cells (b).....	8
-----	---	--	---

499	2	Simulated impedance curves of resonators with $f_1 = 170$ Hz, $f_c = 1350$ Hz,	
500		and varying number of toneholes (thin solid black: cylinder; thick solid grey:	
501		4 holes; thick dashed black: 10 holes; thick solid black: 20 holes). The cutoff	
502		frequency $f_c = 1350$ Hz was chosen to occur at an impedance minimum so that	
503		the effect on the next maximum can be more easily distinguished. Lattices	
504		with 10 holes exhibit very strong cutoff behavior.	10
505	3	Multiple simulated input impedances for resonators with acoustically regular	
506		lattices and random cell orders (50 permutations). The target frequencies are	
507		$f_1 = 170$ Hz and $f_c = 1350$ Hz.	12
508	4	Input impedance of $\mathcal{R}_{1.0}$ (a) and $\mathcal{R}_{2.0}$ (b). Grey: TMM simulation; dashed	
509		black: TMMI simulation; solid black: experimental.	12
510	5	Synthesized (dimensionless) pressure (top) and flow (bottom) inside mouth-	
511		piece for resonators $\mathcal{R}_{1.0}$ (solid black), $\mathcal{R}_{1.5}$ (dash-dot gray), and $\mathcal{R}_{2.0}$ (dashed	
512		black) in the time (left) and frequency (right) domains. Control parameters	
513		are $\gamma = \zeta = 0.45$, and reed resonance $f_r = 1500$ Hz.	20
514	6	Synthesized playing frequency in cents, normalized by the first impedance	
515		peak frequency, for resonators $\mathcal{R}_{1.0}$, $\mathcal{R}_{1.5}$, and $\mathcal{R}_{2.0}$ with solid black, solid	
516		grey, dashed black lines, respectively.	21
517	7	Synthesized spectral centroid, normalized by the playing frequency, for res-	
518		onators $\mathcal{R}_{1.0}$, $\mathcal{R}_{1.5}$, and $\mathcal{R}_{2.0}$ with solid black, solid grey, dashed black lines,	
519		respectively.	22

520	8	Synthesized ($\zeta = 0.45$, $\gamma = 0.55$) spectra of the mouthpiece pressure for	
521		resonators $\mathcal{R}_{1.0}$, $\mathcal{R}_{1.5}$, and $\mathcal{R}_{2.0}$ for 20 fundamental frequencies ranging chro-	
522		matically from 110 Hz to 330 Hz. Odd and even harmonics denoted by squares	
523		and circles, respectively.	23
524	9	Time averaged intensity passing through the entrance of the resonator (left)	
525		and the summed over ten toneholes and exit of resonator (right). Resonators	
526		and synthesis control parameters are the same as in Fig 8. The cutoff fre-	
527		quency for each set of resonators is marked by a vertical line.	26
528	10	Synthesized pressure waveform and sum of time evolving harmonics for res-	
529		onator $\mathcal{R}_{1.0}$ with 5% and 95% thesholds marked.	27
530	11	Synthesized attack time normalized by period of playing frequency for res-	
531		onators $\mathcal{R}_{1.0}$, $\mathcal{R}_{1.5}$ and $\mathcal{R}_{2.0}$ with solid black, solid grey, dashed black lines,	
532		respectively. Variation in attack times due to cutoff frequency is generally	
533		less than 10%.	27
534	List of Tables		

535	I	Dimensions for two prototype resonators with the first impedance peak f_1 at	
536		170 Hz and cutoff frequencies f_c at 1000 Hz and 2000 Hz. Simulated and	
537		measured input impedance are provided in Fig. 4.	31
538	II	Frequencies of the first two impedance peaks and inharmonicity of resonators	
539		$\mathcal{R}_{1.0}$, $\mathcal{R}_{1.5}$, and $\mathcal{R}_{2.0}$	32